48th AIAA Aerospace Sciences Meeting Including the New Horizons Forum and Aerospace Exposition
4 - 7 January 2010, Orlando, Florida

AIAA 2010-878

48th AIAA Aerospace Sciences Meeting Including the New Horizons Forum and Aerospace Exposition, 4-7 Jan 2010, Orlando, Florida

Ensemble and Phase-Locked Averaged Loads Controlled by Plasma Duty Cycles

Xuanshi Meng*, Zhixi Guo †
Northwestern Polytechnical University, Xi'an 710072, China
Feng Liu‡, and Shijun Luo§
University of California, Irvine, CA 92697-3975

An experimental study of the active control of vortices over slender forebodies is performed on a 20° circular-cone-cylinder model using a pair of Single-Dielectric-Barrier-Discharge (SDBD) plasma actuators combined with duty-cycle technique. The tests are carried out in a low-turbulence $3.0\ m \times 1.6\ m$ low-speed wind tunnel at an angle of attack of 45°. The Reynolds number based on the cone base diameter is $50,000$. The results consist of measurements of circumferential pressure distributions over eight stations along the cone forebody, including one station using unsteady pressure tappings, under three different modes of controls: plasma-off, plasma port-on or starboard-on, and plasma duty-cycle actuation. The cross-sectional and overall side forces and yawing moments over the cone are calculated from the measured pressures. The ensemble and phase-locked averaged loads at various duty cycles are investigated.

Nomenclature

C_n	=	yawing moment coefficient about cone base, yawing moment/$q_\infty SD$
C_p	=	pressure coefficient
C_Y	=	overall side-force coefficient, overall side force/$q_\infty S$
C_{Yd}	=	ensemble-averaged local side-force coefficient, local side force/$q_\infty d$
c_{Yd}	=	phase-locked averaged local side-force coefficient
D	=	base diameter of circular cone forebody
d	=	local diameter of circular cone forebody
F	=	frequency of a.c. voltage source
f	=	frequency of duty cycle
L	=	length of circular cone forebody
q_∞	=	free-stream dynamic pressure
Re	=	free-stream Reynolds number based on D
S	=	base area of circular cone forebody
T	=	period of duty cycle
t	=	time of duty cycle
U_∞	=	free-stream velocity
V_{p-p}	=	peak-to-peak voltage of a.c. voltage source
w	=	input power of a.c. voltage source
x, y, z	=	body coordinates, x toward base, y toward starboard, right-hand system

*Lecturer, Department of Fluid Mechanics.
†Senior Student, Department of Fluid Mechanics
‡Professor, Department of Mechanical and Aerospace Engineering. Associate Fellow AIAA.
§Researcher, Department of Mechanical and Aerospace Engineering.

α = angle of attack
θ = meridian angle measured from windward generator, positive when clockwise
τ = fraction of time when starboard actuator is on over a duty-cycle period
ψ = phase angle of duty cycle
Ω = reduced angular frequency of duty-cycle, $2\pi fD/U_\infty$

I. Introduction

Proportional lateral control on slender forebodies at high angles of attack is highly needed in aerodynamic design of air vehicles. The fact that the separation vortices over pointed forebodies generate large airloads and are very sensitive to small perturbations near the body apex offers an exceptional opportunity for manipulating them with little energy input to achieve active lateral control of the verhicle in place of conventional control surfaces. It has been found experimentally that unsteady dynamic control techniques are needed to achieve this goal.[1–3]

Recently, Liu et al.[4] reported wind-tunnel experiments that demonstrate nearly linear proportional control of lateral forces and moments over a slender conical forebody at high angles of attack by employing a novel design of a pair of Single-Dielectric-Barrier-Discharge (SDBD) plasma actuators near the cone apex combined with a duty cycle technique. The flow mechanisms were studied using particle image velocimetry and steady and unsteady pressure tappings.[5,6] The unsteady pressures in the plasma duty cycles are investigated here in detail.

Various methods have been used to study unsteady vortex flowfield over bodies. Lamont[7] used miniature pressure tappings for measuring unsteady pressures in addition to the time-averaged pressure tappings to demonstrate that his experimental setup had produced the hoped-for absence of serious flow unsteadiness. Thomas, Kozlov and Corke[8] studied ensemble averaged and phase-locked averaged particle image velocimetry of the flow over a cylinder controlled by plasma duty cycles.

Flow under plasma duty-cycle actuation is naturally unsteady. The reduced angular frequency of duty cycle is of the order of 1. On the other end, the reduced angular frequency range of typical aircraft aerodynamic maneuvers is of the order of 0.01 based on the spectrum of unsteady flow phenomena over delta wings given by Menke, al et.,[9] which is much smaller than that of the plasma duty-cycle. Thus, typical aircraft could not respond the instantaneous (unsteady) loads under plasma duty-cycle actuations but just respond the time-averaged (steady) loads. This observation agrees with the predictions of Hanff et al.[2] Therefore, the ensemble-averaged pressures are useful in aircraft-maneuver design, and the phase-locked averaged pressures are required for flow-mechanism study.

In the following sections, the experimental setup is described. The experinental results are analyzed in the form of ensemble and phase-locked averages. Finally conclusions are drawn.

II. Experimental Setup

The model is that used in Ref. 4, but the installment of the plasma actutors is refined and unsteady pressure tappings are mounted in an additional pressure station. 252 time-averaged pressure tappings, Models 9816 and 8400 by the PSI Company, are arranged in rings of 36, every 10° around the circumference of the cone, at Stations 1 to 7 as shown in Fig. 1. Models 9816 and 8400 are read at frequency of 100 Hz and 127 Hz, respectively. In addition to the time-averaged pressure tappings, ten unsteady pressure tappings, Model $XCQ-093$ by the Kulite Semiconductor Products Inc. are mounted around the circumference of Station 8, Seven tappings are distributed every 30° from $\theta = 90°$ to 270° and the rest three at $\theta = 0°$ and $\pm 50°$. They are measured with sampling frequency of 500 Hz. Input pressure range is 0.35 BAR and perpendicular acceleration sensitivity % FS/g is 1.5×10^{-3}. The Kulite pressure-transducers can operate quick, enabling them to detect very brief, small fluctuations in pressure. Consecutive 15 seconds samplings of all tappings are recorded for analyses.

The model consists two separate pieces. The frontal portion of the cone is made of plastic and has a length of 150 mm. The rest of the model is made of metal. Two long strips of SDBD plasma-actuators are installed symmetrically on the plastic frontal cone near the apex as shown in Fig. 2(a). The plasma actuator consists of two asymmetric copper electrodes each of 0.03 mm thickness. A thin Kapton dielectric

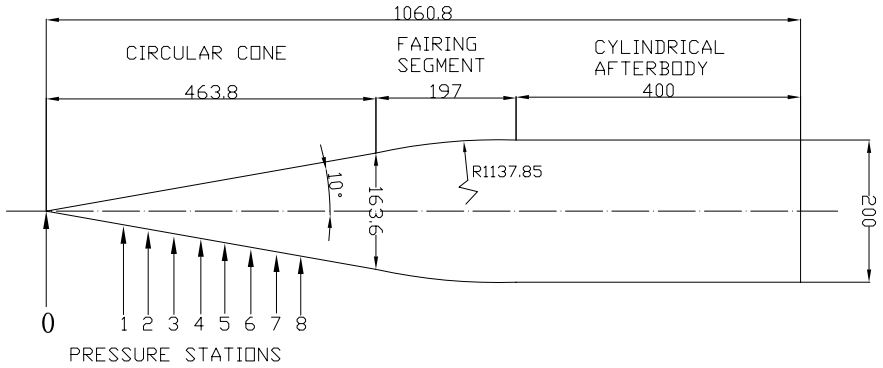

0-1	0-2	0-3	0-4	0-5	0-6	0-7	0-8
166.8	201.9	236.9	272.0	307.1	342.1	377.2	412.2

DIMENSIONS IN mm

Figure 1. The model

film wraps around the cone surface and separates the encapsulated electrode from the exposed electrode as shown in Fig. 2(b). The right edge of the exposed electrode shown in Fig. 2(b) is aligned with the cone at the azimuth angle $\theta = \pm 120°$, where θ is measured from the windward meridian of the cone and positive is clockwise when looking upstream (Fig. 2(a)). The length of the electrodes is 20 mm along the cone meridian with the leading edge located at 9 mm from the cone apex. The width of the exposed and encapsulated electrode is 1 mm and 2 mm, respectively. The two electrodes are separated by a gap of 1.5 mm, where the plasma is created and emits a blue glow in darkness. The plasma-actuator arrangement is intended to affect the boundary-layer separation positions on the cone surface. Care is taken in manufacturing and mounting of the frontal cone to the rear portion of the model to make sure they are well aligned. The actuators are hand-made and attached directly to the cone surface with no allowance.

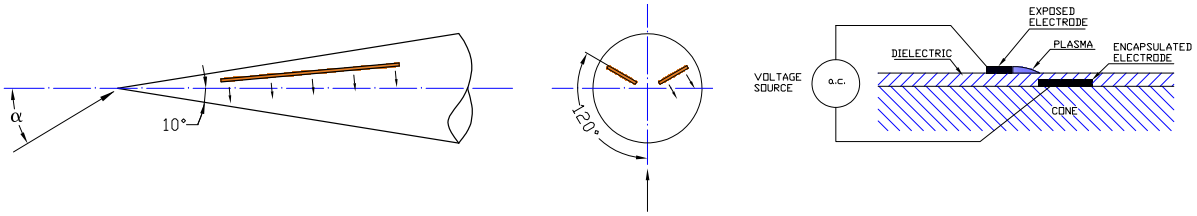

(a) arrangement (b) SDBD

Figure 2. Sketches of the plasma actuators.

Three modes of operations of the actuators are defined. The plasma-off mode corresponds to the case when neither of the two actuators is activated. The plasma-on mode refers to the conditions when either the port or starboard actuator is activated while the other is kept off during the test. These are called the port-on and starboard-on modes, respectively. Each of the two actuators on the cone model is separately driven by an a.c. voltage source (model CTP-2000K by Nanjing Suman Co.). The waveform of the a.c. source is sine wave. The peak-to-peak voltage and frequency are set at $V_{p-p} \approx 14\ kV$ and $F \approx 8.9\ kHz$,

respectively. The measured power consumption is $w \approx 19.3\ W$. The third mode employs a duty-cycle technique in which the two actuators on the cone is activated alternately with a specified duty cycle, τ, defined as the fraction of time when the starboard actuator is on over a duty-cycle period. The fraction of time that the port actuator is on is then $1 - \tau$. The duty cycles are achieved by modulating the carrier a.c. voltage sources by a digital pulse wave generator, PC-07 made by the Nanjing Suman Co, at a frequency of 10 Hz which yields a reduced angular frequency, $\Omega \approx 2$.The input power for the plasma duty cycle has a minimum, $w_{min} \approx 10.5\ W$ at $\tau = 50\%$, and a maximum, $w_{max} \approx 23.0\ W$ at $\tau = 10\%$ and 90%.

The tests are conducted in an open-circuit low-speed wind tunnel at Northwestern Polytechnical University. The test section has a $3.0\ m \times 1.6\ m$ cross section. The cone-cylinder model is tested at $\alpha = 45°$. The free-stream velocity $U_\infty = 5\ m/s$. The Reynolds number based on the cone base diameter is 5×10^4. The model is rigidly mounted on a support from the starboard side of the model aft-cylinder as shown in Fig. 3. The support is fixed onto the turning plate of angle of attack inbedded in the bottom wall of the wind-tunnel test-section. The model support is not symmetric with respect to the incidence plane of the model and, thus, would have an asymmetric interference on the flow around the cone forebody. Local and overall side force, and yawing moment are calculated from the measured pressures. The local side-force coefficient C_{Yd} is normalized with the local diameter d and is positive when pointing to the starboard side of the cone. The yawing moment coefficient C_n is taken about the cone base and positive when yawing to the starboard side, and normalized with the base diameter D and base area S. The model is carefully cleaned prior to each run of the wind tunnel.

Figure 3. Model in the wind tunnel, leeward view

III. Base Plasma-Off Flow at Zero Angle of Attack

In order to check the accurary of the model setup in the wind tunnel, a test is run at zero angle of attack and with plasma off. Fig. 4 presents the ensemble-averaged pressure distributions over the circumference of Stations $1 - 7$ at $\alpha = 0°$ and $U_\infty = 5\ m/s$. Aside from some slight irregularities, the measured pressure distributions indicate essentially an axisymmetric flow around the cone.

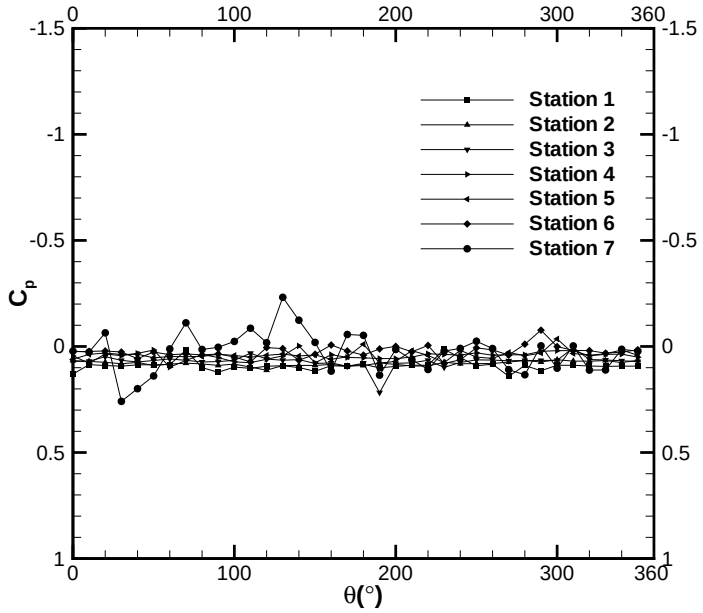

Figure 4. Ensemble-averaged pressure distributions over various stations for plasma off at $\alpha = 0^\circ$ and $U_\infty = 5\ m/s$.

IV. Variation of Ensemble-Averaged Pressures with Sampling Time

To study the convergence rate of the ensemble averages, the pressure measurements by unsteady pressure tappings on Station 8 are studied. Figures 5, 6 and 7 compare the ensemble-averaged pressure distributions at Station 8 obtained with sampling times of 1 s,,5 s, 10 s and 15 s at various duty cycles for $\tau = 0.1-0.3, 0.4-0.6$ and $0.7-.0.9$, respectively. The ensemble-averaged pressure distribution at a given plasma duty cycle becomes almost invariant as the averaging time is greater than 1 s. Flow under plasma duty-cycled control is naturally unsteady. On Station 8 the pressures are measured by Kulite transducers. The Kulite pressure-transducer measurement with sampling frequency of 500 Hz can detect very brief, small fluctuations in pressure. In 1 s, Kulite pressure-transducer measurements cover 10 plasma duty cycles & 50 times per duty cycle. Thus, the ensemble-averaged pressure may approach a limit, and the flow under the plasma duty-cycled control could be considered steady when the averaging time is greater than 1 s. Therefore, typical aircraft under the plasma duty-cycled control would respond the steady, ensemble-averaged loads rather than unsteady, instantaneous loads.

Pressures on Stations $1-7$ are measured by time-averaged pressure tappings. The ensemble averaged pressure converges even when the sampling time is lower than 1 s (not shown here for brevity). We will present the 15 s averaged data next except otherwise stated.

V. Ensemble-Averaged Pressures, Lateral Forces and Moments

Figure 8 presents the ensemble averaged pressure distributions on even-numbered Stations at $\alpha = 45^\circ$, $U_\infty = 5\ m/s$ for varius cases, where OFF denotes that plasma is off, $\tau = 0$ and 1 denote that the port- and starboard-side plasma actuator is on, respectively, and $\tau = 0.1-0.9$ denote plasma duty cycles. For port-on ($\tau = 0$), the higher suction peak appears on the starboard side of the cone. For starboard-on ($\tau = 1$), the higher suction peak moves onto the port side. The two pressure distributions are nearly anti-symmetric with each other. For various duty cycles ($\tau = 0.1-0.9$), the pressure distributions change continuously from that of port-on to that of starboard-on. The pressure distributions for τ, and $1-\tau$ are almost anti-symmetric, and become symmetric for $\tau = 0.5$. The results on the odd-numbered Stations are similar (not shown here

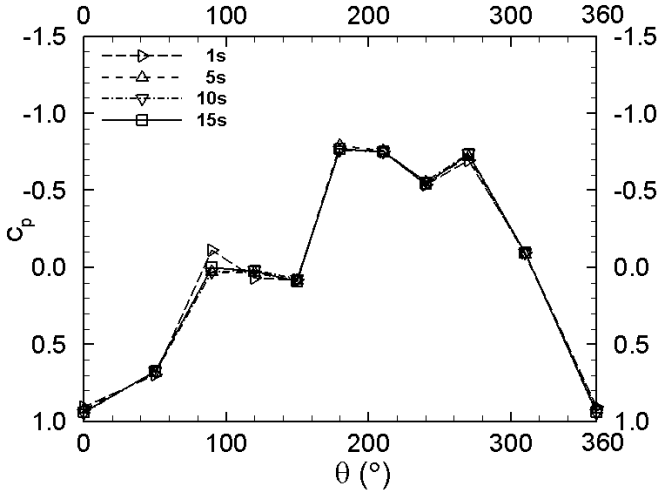

(a) $\tau = 0.1$

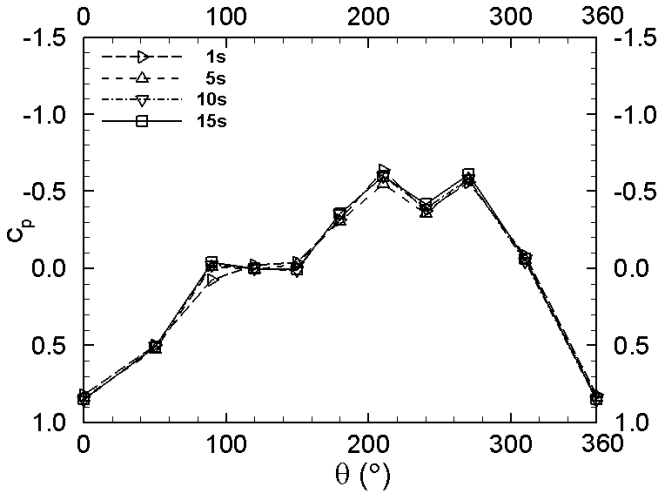

(b) $\tau = 0.2$

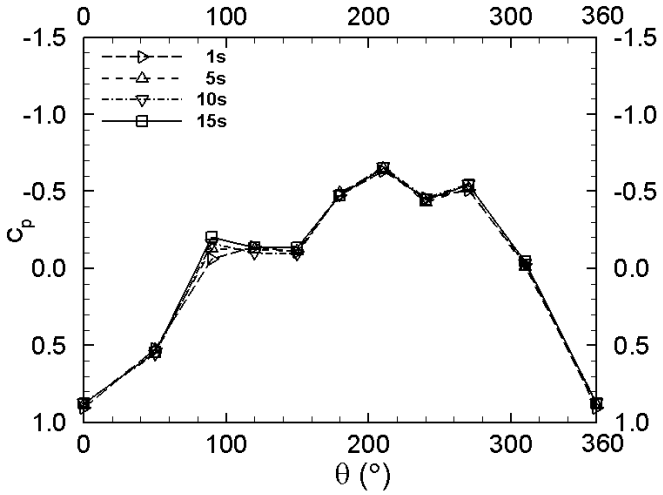

(c) $\tau = 0.3$

Figure 5. Pressures ensemble-averaged over $1\ s$, $5\ s$, $10\ s$ **and** $15\ s$, $\tau = 0.1 - 0.3$, **Station** 8, $\alpha = 45°$.

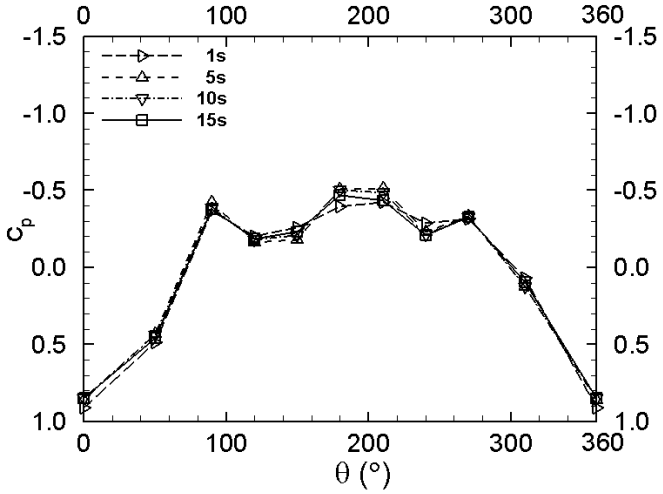

(a) $\tau = 0.4$

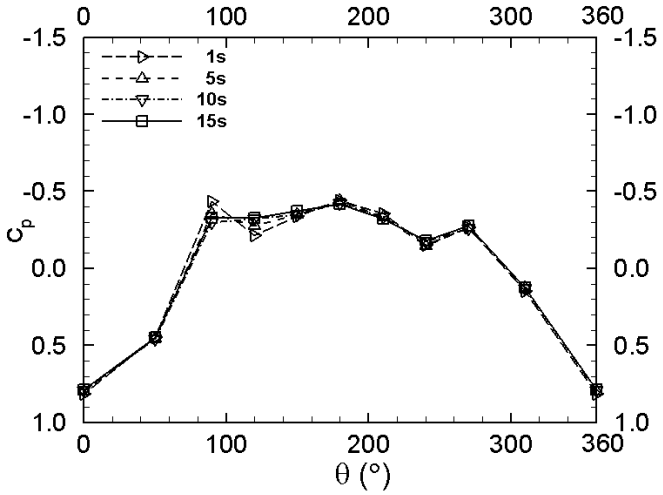

(b) $\tau = 0.5$

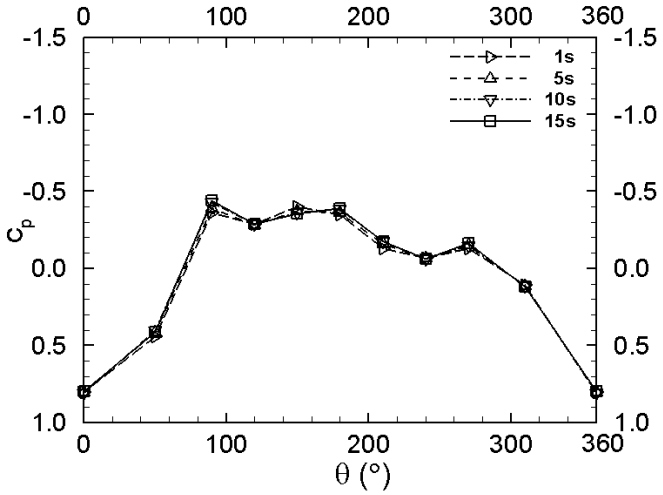

(c) $\tau = 0.6$

Figure 6. Pressures ensemble-averaged over $1\ s$, $5\ s$, $10\ s$ **and** $15\ s$, $\tau = 0.4 - 0.6$, **Station** 8, $\alpha = 45°$.

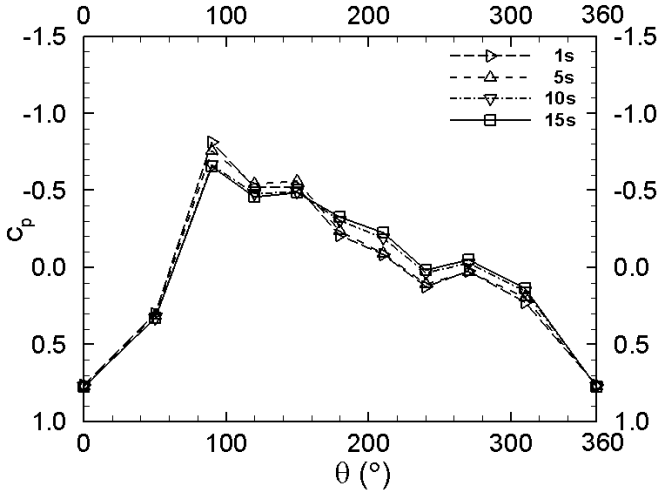

(a) $\tau = 0.7$

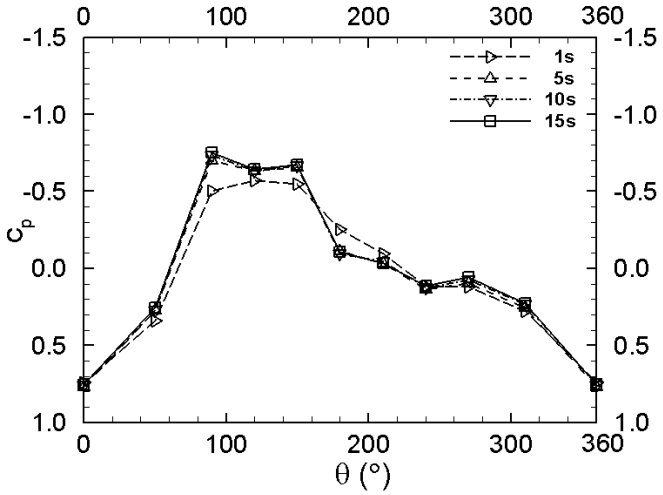

(b) $\tau = 0.8$

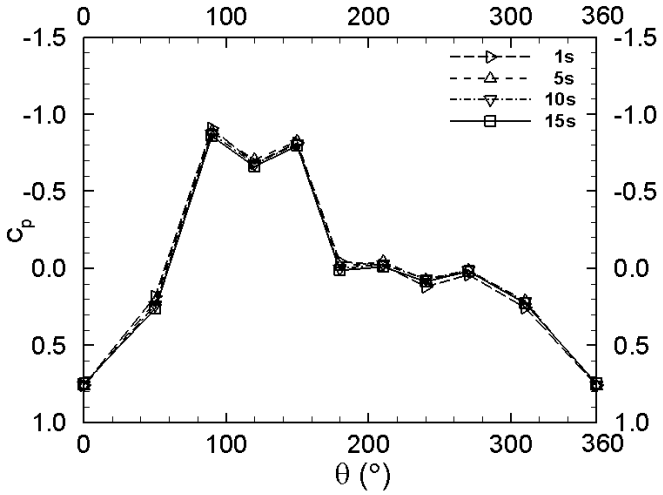

(c) $\tau = 0.9$

Figure 7. Pressures ensemble-averaged over $1\ s$, $5\ s$, $10\ s$ **and** $15\ s$, $\tau = 0.7 - 0.9$, **Station** 8, $\alpha = 45°$.

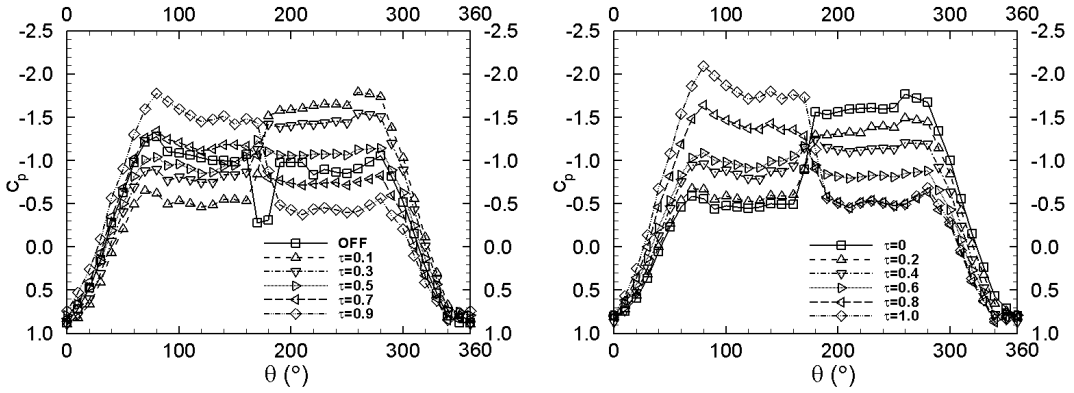

(a) Station 2

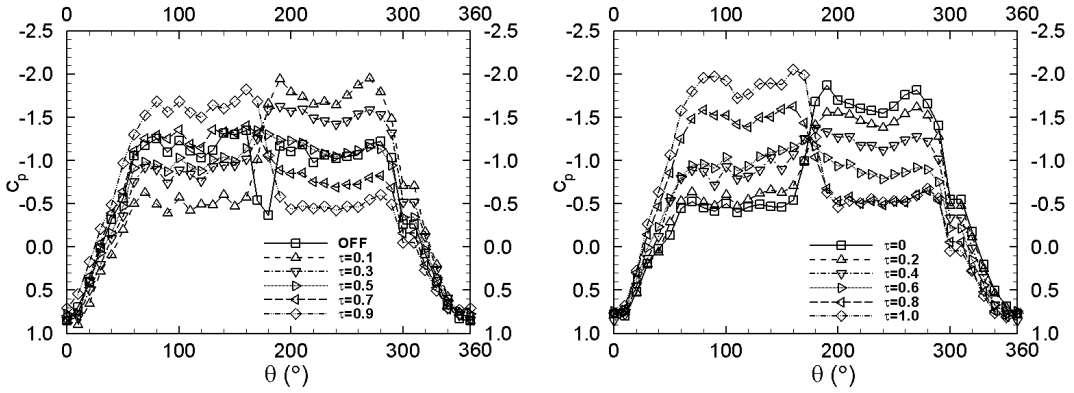

(b) Station 4

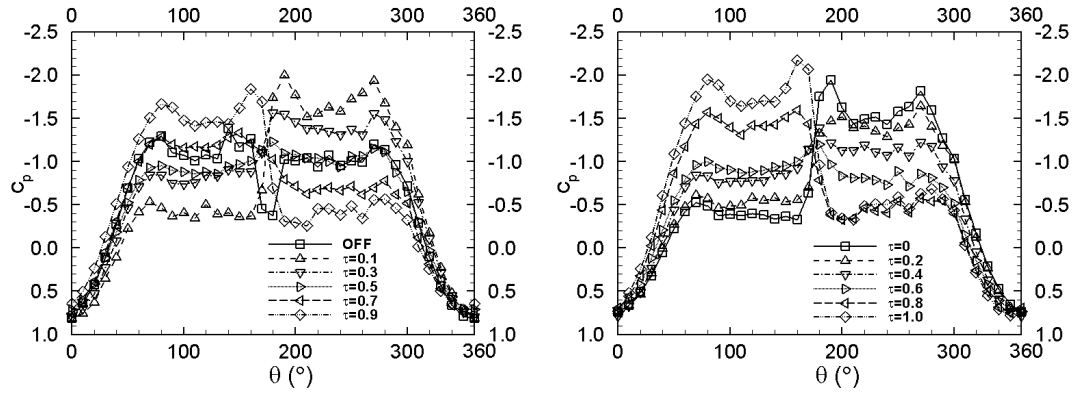

(c) Station 6

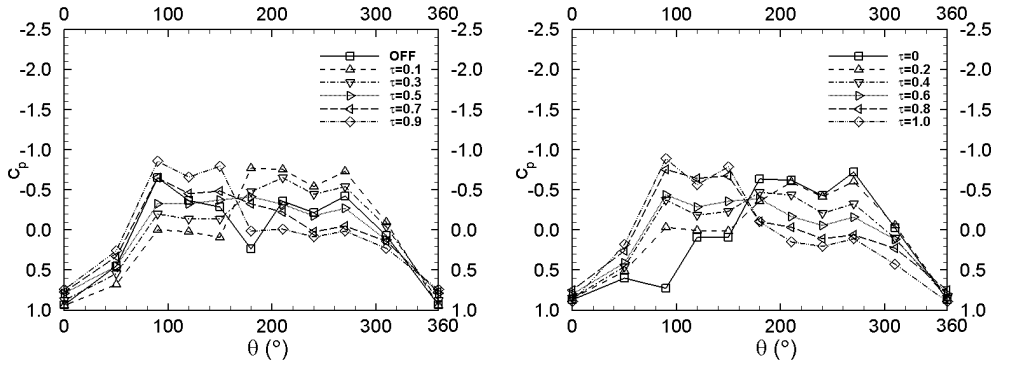

(d) Station 8

Figure 8. Comparison of ensemble-averaged pressures for various duty cycles, even Stations, $\alpha = 45°$.

for brevity). The pressure distributions on Station 8 are similar to other Stations at a given τ, but the suction peaks on Station 8 are relatively lowered. This may be caused by that there are only 10 pressure tappings mounted over Station 8, whereas 36 tappings on each of Stations $1-7$. Nevertheless, the essential features of the pressure distribution on Station 8 are depicted..

For plasma-off, the pressure distribution happens incidentally to be nearly symmetric. The resulting side force nearly vanishes rather than takes the maximum positive or negative values of bi-stable states. Such result was reported in the literature. For example, by force measurement Zilliac et al.[10] showed that for a slender ogive-cylinder body at high angles of attack the side force most likely takes one of the two extreme values, but there exist few cases in which the side force equals to an intermediate value, including zero.

Several wind tunnel runs of the same model were performed over a period of nine months. For port-on and starboard-on the pressure asymmetry remains unchanged, but for plasma-off, different pressure asymmetries are observed. The presure distribution for plasma-off is close to that under port-on by Fig. 3 of Ref. 4 and close to that under starboard-on by Fig. 9 in Ref. 5. In fact, for plasma-off, force asymmetry over slender body of revolution at high angles of attack depends on small asymmetric disturbances in the flow, including the micro surface imperfections on the tip of the body.

Ensemble-averaged local and overall side force and yawing moment are calculated from the ensemble averaged pressures. Figures 9 and 10 present ensemble-averaged local side force C_{Yd} versus x/L and τ, respectively, at $\alpha = 45°$, $U_\infty = 5\ m/s$. The values C_{Yd} at $\tau = 0$ and $\tau = 1.0$ are taken from those of the port-on and starboard-on, respectively. Fig. 10 shows that proportional control of asymmetric force is achieved by the duty-cycled plasma actuations. In both figures, the values of C_{Yd} on Station 8 match well with those on other Stations, which shows that the fewer pressure tappings on the Station 8 are tolerable. Fig. 11 gives the overall side force coefficient C_Y and yawing moment coefficient C_n versus duty cycle τ at $\alpha = 45°$, $U_\infty = 5\ m/s$. Here, the pressure data on Stations $1-7$ are used, and those on Station 8 are used because of slight inaccuracy. The linearity of the side force and yawing moment with respect to the duty cycle is improved over previous studies[4] due to the improved design of the actuators.

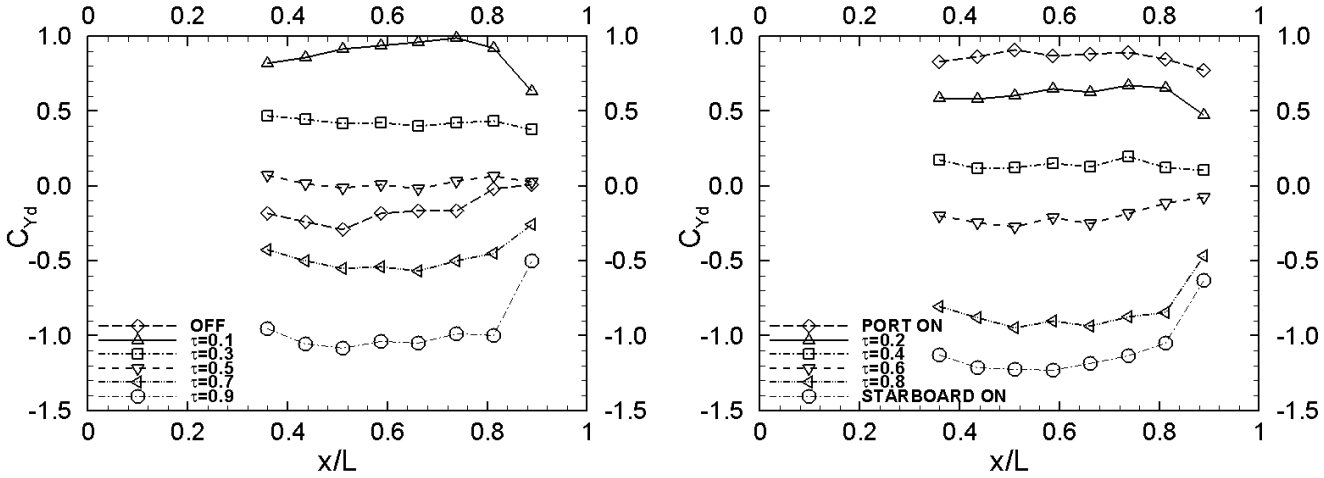

Figure 9. Ensemble-averaged local side force vs. x/L, $\alpha = 45°$.

VI. Phase-Locked Local Side Force on Station 8

The mechanisms of the plasma-duty-cycled flow are investigated by phase-locked (locked to the plasma duty cycle) averaged pressures and side force. The time-averaged pressure tappings can not resolve the phase-locked pressures produced by the plasma duty cycle due to their pressure acquisition technique. Thus, only the local pressure distribution and local side force on Station 8 is considered here. The pressure distribution over Station 8 are measured by the Kulite unsteady- pressure-transducers. The Kulite sampling has a rate of 500 Hz and is taken consecutively for 15 s in each test. The frequency of duty cycle is 10 Hz. In one period of the duty cycle there are 50 readings evenly distributed at phase-angle increment of 7.2°. At a given

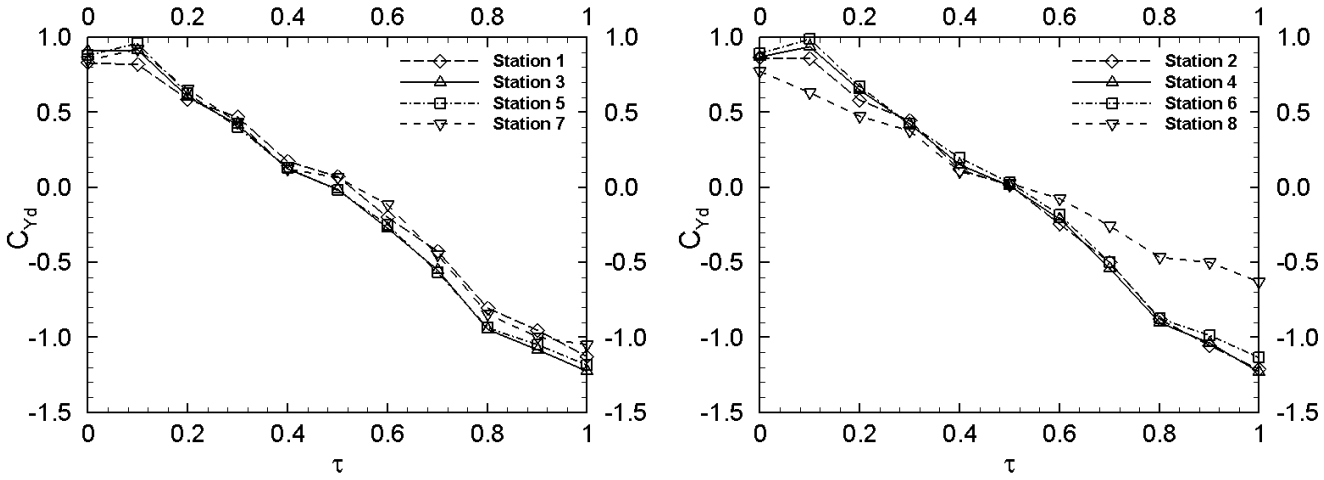

Figure 10. Ensemble-averaged local side force vs. duty cycle, $\alpha = 45°$.

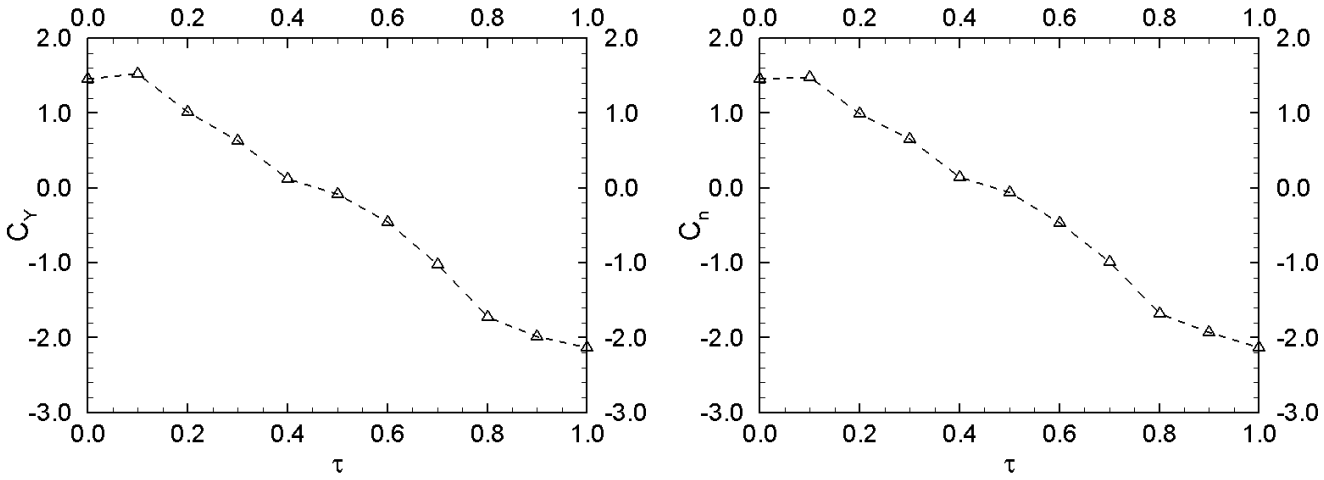

Figure 11. Ensemble-averaged overall side force and yawing moment vs. duty cycle, $\alpha = 45°$.

phase angle there are totally 150 samples to be averaged in the sampling time of 15 s.

Figures 12 to 14 show convergence of the phase-locked averaged local side force coefficient c_{Yd} with sampling time from 1 s to 15 s at duty cycle $\tau = 0.1 - 0.9$. It is seen that the curve c_{Yd} versus time t almost converges to a limit at the sampling time of 15 s. The time of $t/T = 0$ is set, by estimation, at the beginning of the port-side plasma actuation. The corresponding ensemble averaged local side force coefficient C_{Yd} obtained from Fig. 10 is shown by dotted line in the figures. The ensemble averaged C_{Yd} is the time average of the converged phase-locked averaged $c_{Yd}(t)$ over a period of the plasma duty cycle. We will discuss the 15 s averaged phase-locked data next.

The variation of the phase-locked local side force c_{Yd} with time t follows the alternate activations of the port-side and starboard-side plasma actuators in a given period of the duty cycle. The variation of the phase-locked averaged side force with time, $c_{Yd}(t)$ for a given duty cycle is a smooth-wave curve. It is not the square-wave curve predicted by Hanff et al.[2] in their Figure 2(a) and also by Nelson et al.[11] Furthermore, the maximum and minimum values of the phase-locked averaged side force $c_{Yd}(t)$ are not the ensemble averaged side forces C_{Yd} of port-on and starboard-on.[2,11] The reason for the deviations is that the plasma duty-cycled flow is inherently unsteady, while the flows under plasma port-on and starbaord-on are practically steady. The smooth-wave curve of $c_{Yd}(t)$ has about five oscillations in a period of the plasma duty cycle at a given duty cycle. The oscillation is weak when the duty cycle closes the two extremes 0.1 and 0.9 and becomes strong when the duty cycle approaches 0.5. As $\tau \approx 0.1$ and 0.9, one of the two opposite plasma actuations is dominant. It is the dominant actuation to determine the flow and small flow oscillations may prevail. When τ approaches 0.5, the two opposite plasma actuations are about of equal duration and a strong cancellation occurs, which may result in the large flow oscillations. This phenomena may be related to the variation of the input power with duty cycle. The input power is maximum at $\tau = 0.1$ and 0.9, minimum at $\tau = 0.5$, and medium for $\tau = 0$ and 1. (See Section 2.) Why the number of side-force oscillations in a period of plasma duty cycle is five is unclear to the present authors.

VII. Phase-Locked-Averaged Pressures on Station 8

Figures 15-17 present the phase-locked-averaged pressure distributions at five evenly distributed phase angles $\psi = 0°, 72°, 144°, 216°$, and $288°$, compared with the ensemble-averaged pressure distributions at Station 8 and $\alpha = 45°$. The 15 s phase-locked averaged pressures are presented here. The mean of the phase-locked-averaged pressure at the five phase angles is, in general, not the ensemble averaged pressure at a given meridian angle θ, since the latter is the average over all phase angles. Overall, the variation of the phase-locked averaged pressure distribution with phase angle matches with the alternate activations of the port-side and starboard-side actuators. The variation of the phase-locked pressure coefficient C_p with meridian angle θ is oscillatory at certain duty cycles. There appear 3 oscillations in a period of the plasma duty cycle. Three oscillating suction peaks at $\theta = 90°, 180°$ and $270°$ are distinctly observed at a given phase angle at $\tau = 0.2, 0.3, 0.5$ and 0.6. The oscillations disappear when $\tau = 0.1$ and 0.9, and the phase-locked averaged pressure distribution almost coincides with the ensemble averaged pressure distribution. At the rest values of the duty cycle the situation is intermediate. The phenomena may be due to the interactions between the two opposite plasma actuations in the duty cycle.

Although only ten Kulite unsteady pressure transducers are mounted around the circumference of Station 8, the essential unsteady characteristics of the plasma duty-cycled flow are clearly depicted. It is expected that the aerodynamic features obtained from Station 8 would be true for the entire circular-cone forebody.

VIII. Conclusions

The results of the present paper reconfirm previous findings that it is possible to achieve linear proportional control of the lateral forces and moments of a slender circular-cone body by the duty-cycled plasma flow control technique with appropriately designed plasma actuators and selected electric parameters. The linearity of the controlled lateral forces and moments with respect to the duty cycle is improved over previous studies because of the improved design of the actuators.

Through analyzing the pressure data obtained by time-averaged and unsteady pressure tappings, the following flow features are revealed.

1. The ensemble-averaged pressure at a given point approaches a constant when the sampling time is over

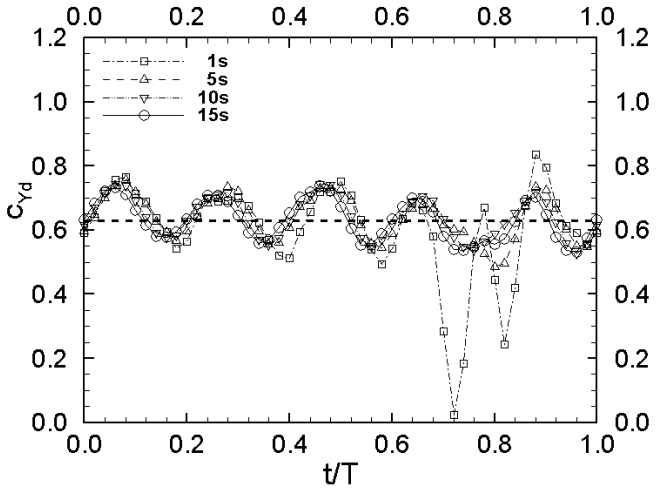

(a) $\tau = 0.1$

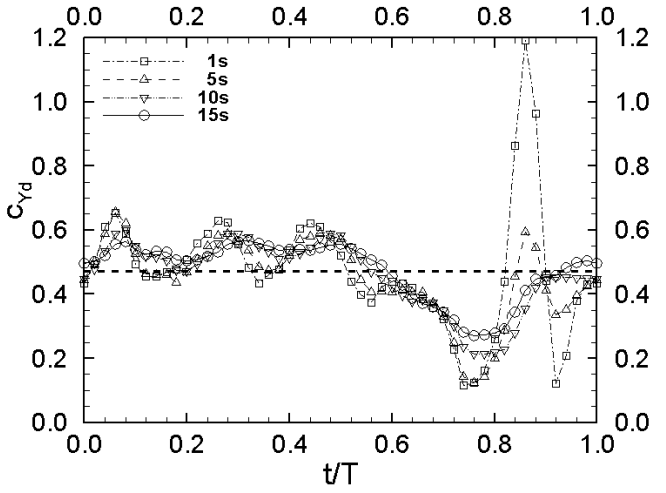

(b) $\tau = 0.2$

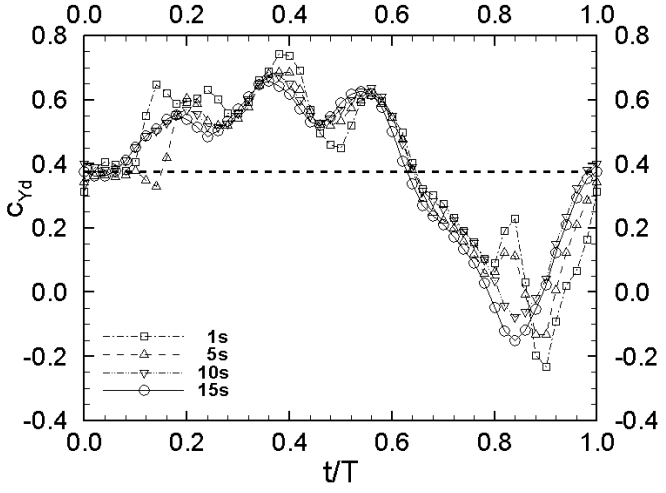

(c) $\tau = 0.3$

Figure 12. Local side force phase-locked averaged over $1\ s - 15\ s$ compared with ensemble-averaged side force (dotted line), $\tau = 0.1 - 0.3$, Station 8, $\alpha = 45°$.

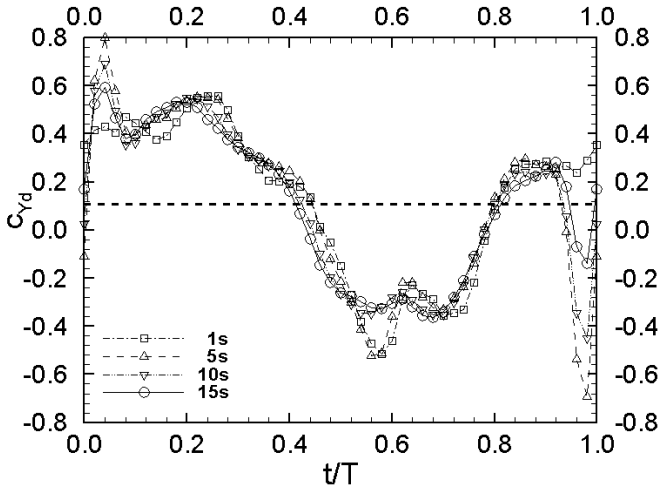

(a) $\tau = 0.4$

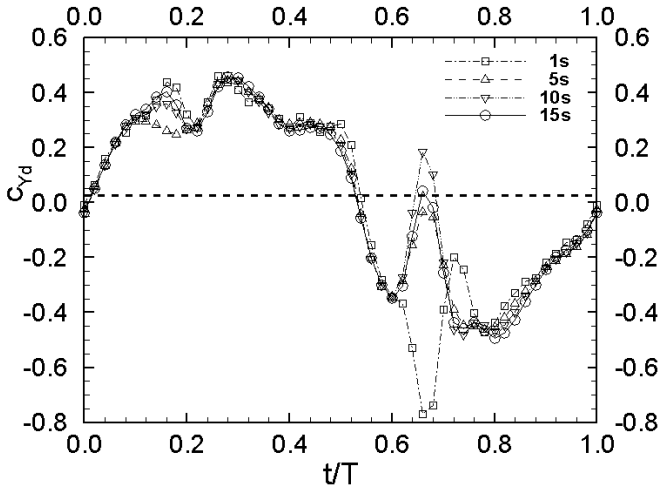

(b) $\tau = 0.5$

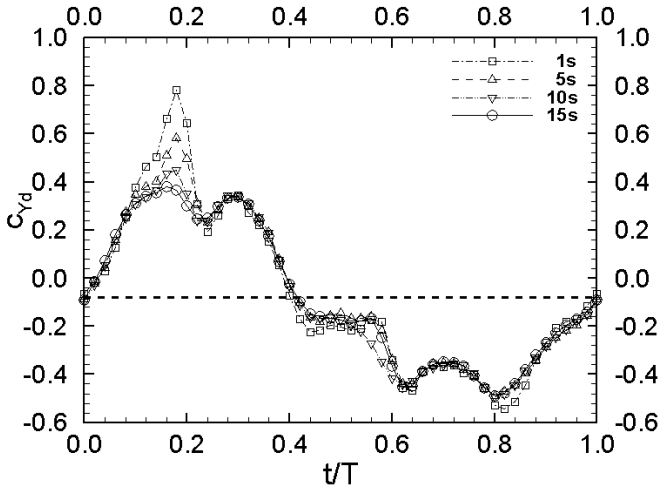

(c) $\tau = 0.6$

Figure 13. Local side force phase-locked averaged over $1\ s - 15\ s$ **compared with ensemble-averaged side force (dotted line),** $\tau = 0.4 - 0.6$**, Station** 8**,** $\alpha = 45°$**.**

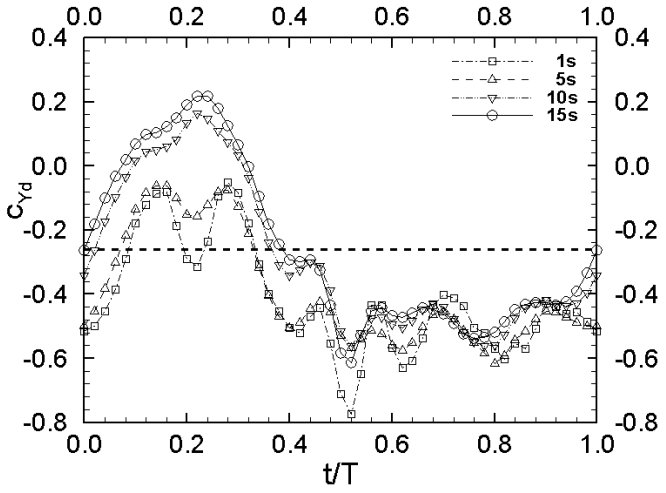

(a) $\tau = 0.7$

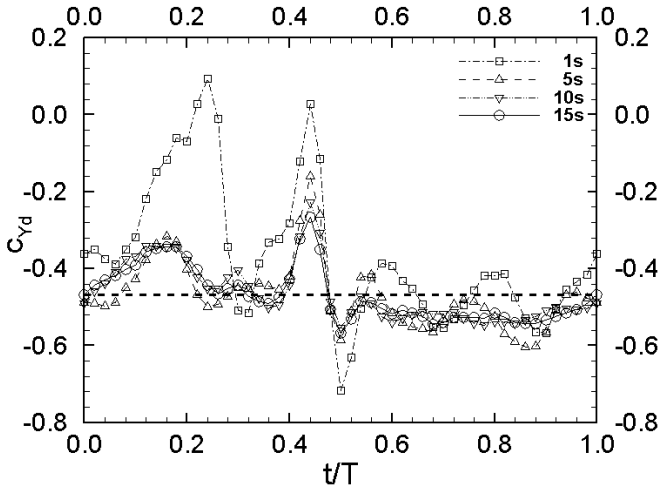

(b) $\tau = 0.8$

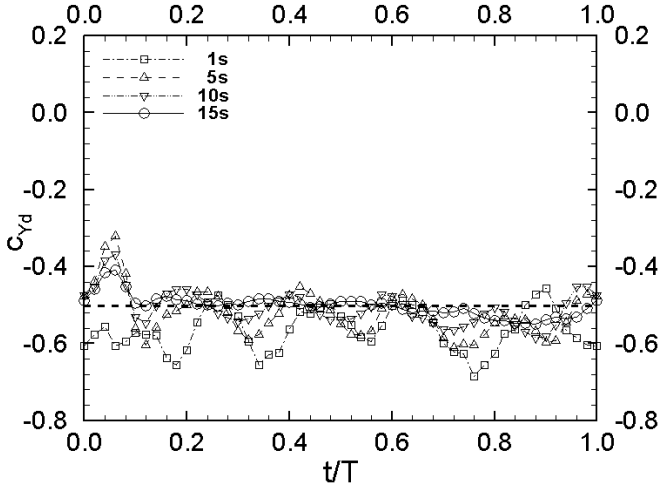

(c) $\tau = 0.9$

Figure 14. Local side force phase-locked averaged over $1\ s - 15\ s$ compared with ensemble-averaged side force (dotted line), $\tau = 0.7 - 0.9$, Station 8, $\alpha = 45°$.

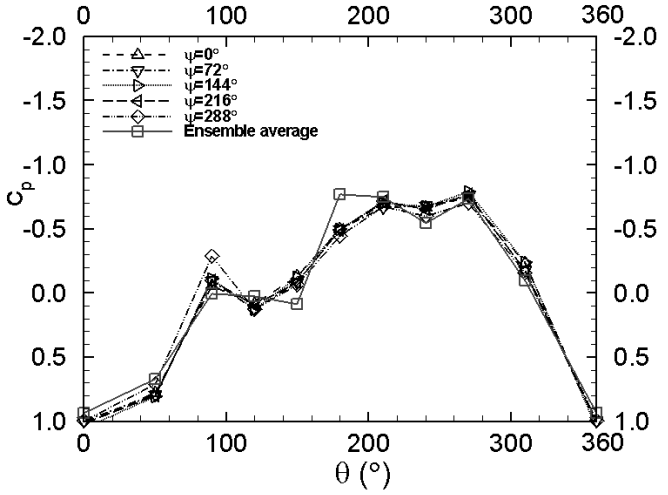

(a) $\tau = 0.1$

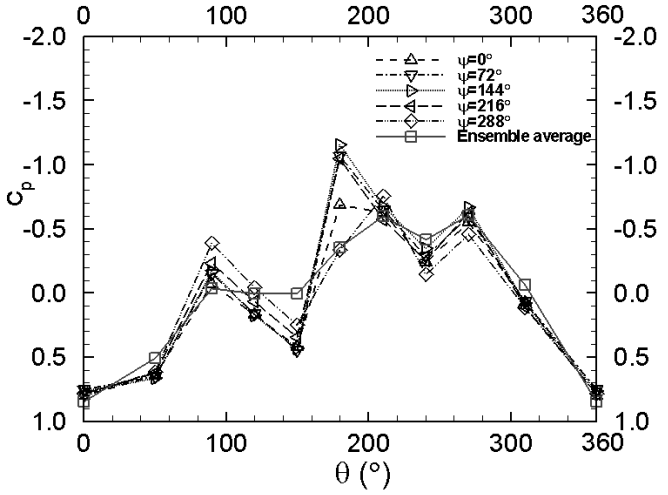

(b) $\tau = 0.2$

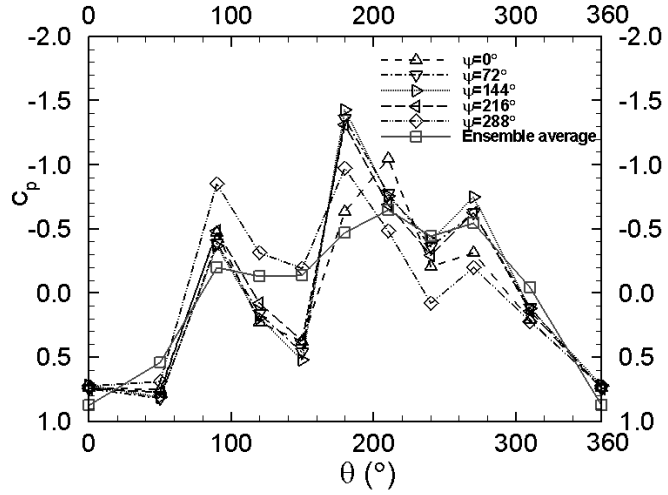

(c) $\tau = 0.3$

Figure 15. Phase-locked-averaged pressures compared with ensemble-averaged pressures, $\tau = 0.1 - 0.3$, Station 8, $\alpha = 45°$.

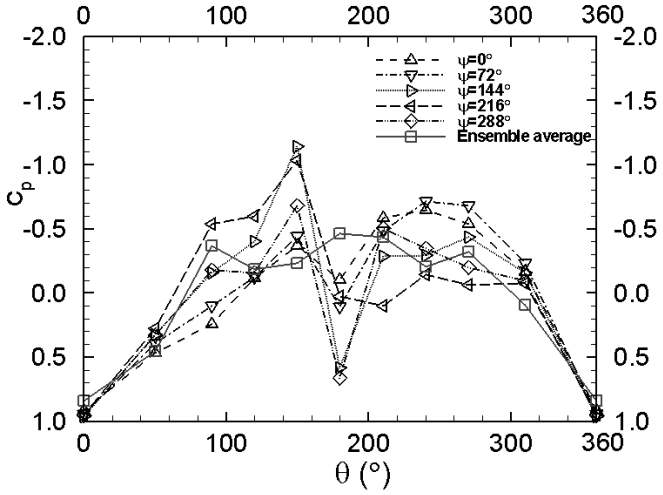

(a) $\tau = 0.4$

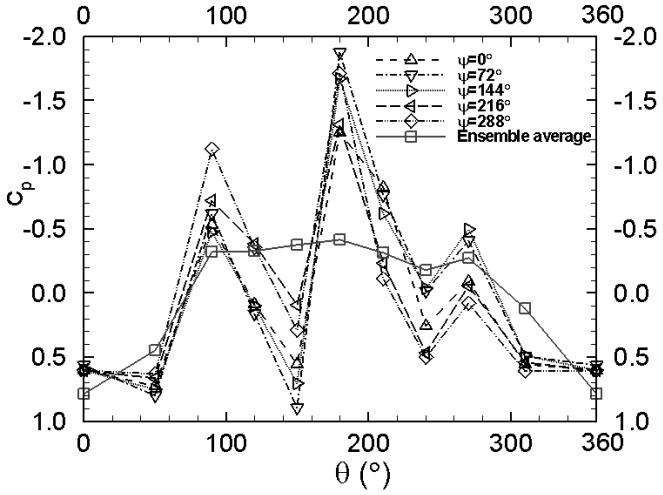

(b) $\tau = 0.5$

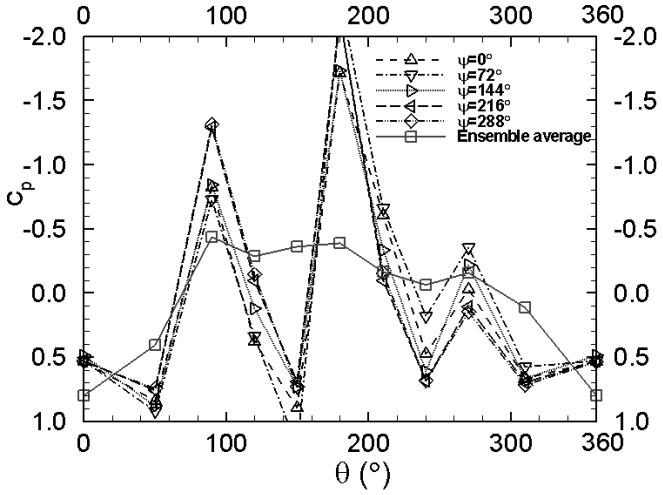

(c) $\tau = 0.6$

Figure 16. Phase-locked-averaged pressures compared with ensemble-averaged pressures, $\tau = 0.4 - 0.6$, Station 8, $\alpha = 45°$.

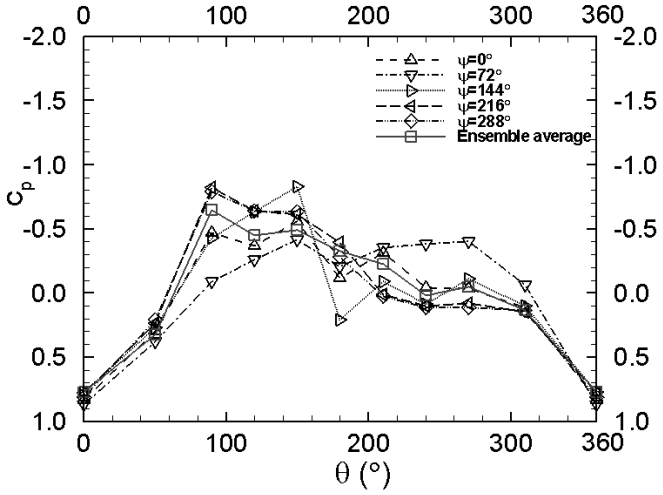

(a) $\tau = 0.7$

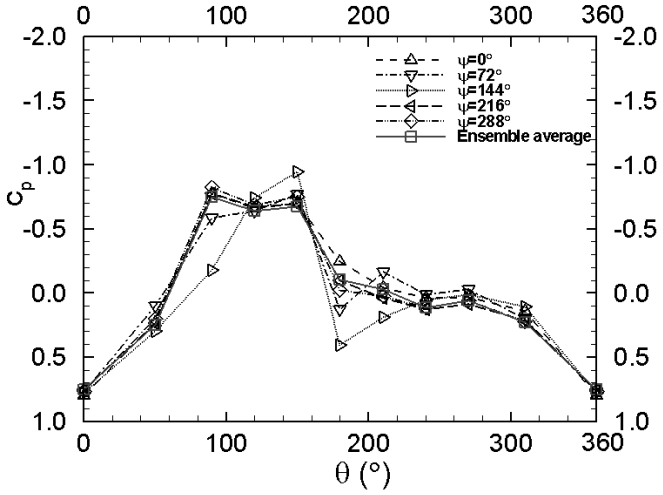

(b) $\tau = 0.8$

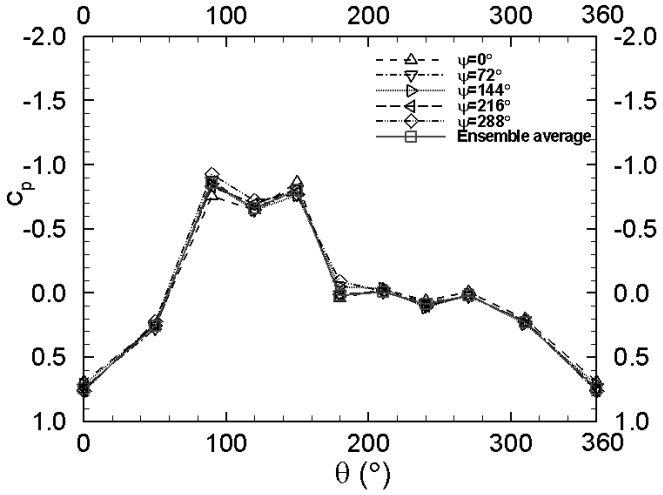

(c) $\tau = 0.9$

Figure 17. Phase-locked-averaged pressures compared with ensemble-averaged pressures, $\tau = 0.7 - 0.9$, Station 8, $\alpha = 45°$.

one second.

2. The ensemble-averaged pressure distribution over the cone forebody at a given duty cycle is essentially conical at angle of attack of 45°.

3. The phase-locked-averaged side force approaches to a limit when the sampling time is 15 seconds at a given phase angle.

4. The phase-locked-averaged side force oscillates around the ensemble-averaged side force five times in a period of the duty cycles.

5. The phase-locked-averaged pressure versus meridian angle oscillates three times over the circumference of a cross section at certain duty cycles.

6. The oscillations in Item 4 and 5 are strong when the duty cycle approaches 50%, and weak as the duty cycle closes 10% and 90%, while the input power of the a.c. voltage source is lowest and highest, respectively.

7. The variation of the phase-locked-averaged side force with time in a period of the duty cycle is a smooth-wave curve rather than the square-wave curve predicted in literatures.

8. The maximum and minimum values of the phase-locked-averaged side force over a period of the duty cycle are not those produced by the port- and starboard-side actuator alone.

9. Typical aircraft motion would respond the ensemble-averaged loads (stationary loads), but could not respond the phase-locked-averaged loads (unsteady loads), as the reduced frequency of the duty cycle is much larger than that of aircraft motion.

A repetition test with the unsteady-pressure sampling-time more than 15 seconds to investigate Itemes $3-6$ in detail is suggested.

Acknowledgments

The present work is supported by the Foundation for Fundamental Research of the Northwestern Polytechnical University, NPU-FFR-W018101 and the Specialized Research Fund for the Doctoral Program of Higher Education, SRFDP-200806990003.

References

[1]Bernhardt, J. E. and Williams, D. R., "Proportional control of asymmetric forebody vortices," *AIAA Journal*, Vol. 36, No. 11, Nov. 1998, pp. 2087–2093.

[2]Hanff, E., Lee, R., and Kind, R. J., "Investigations on a dynamic forebodey flow control system," Proceedings of the 18th International Congress on Instrumentation in Aerospace Simulation Facilities, Inst. of Electrical and Electronics Engineers, Piscataway, NJ, 1999, pp. 28/1-28/9.

[3]Ming, X. and Gu, Y., "An innovative control technique for slender bodies at high angle of attack," AIAA Paper 2006-3688, June 2006.

[4]Liu, F., Luo, S.J.,Gao, C., Meng, X.S., Hao, J.N., Wang, J.L. and Zhao, Z.J., "Flow control over a conical forebody using duty-cycled plasma actuators," *AIAA Journal*, Vol. 46, No. 11, Nov. 2008, pp. 2969–2973.

[5]Liu, F., Luo, S.J.,Gao, C., Wang, J.L., Zhao, Z.J, Li, Y.Z. and Hao, J.N., "Mechanisms for conical forebody flow control using plasma actuators," AIAA Paper 2009-4284, June 2009.

[6]Wang, J.L., Li, H.X., Liu, F. and Luo, S.J., "PIV study on forebody vortex cores under plasma actuations," AIAA Paper 2010-1087, Jan. 2010.

[7]Lamont, P.J., "Pressure around an inclined ogive cylinder with laminar, transitional, or turbulent separation," *AIAA Journal*, Vol. 20, No. 11, Nov. 1982, pp. 1492–1499.

[8]Thomas, F.O., Kozlov, A. and Corke, T.C., "Plasma actuators for cylinder flow control and noise reduction," *AIAA Journal*, Vol. 45, No. 8, Aug. 2008, pp. 1921–1931.

[9]Menke, M., Yang, H. and Gursul, I., "Experiments on the unsteady nature of vortex breakdown over delta wings," *Experiments in Fluids*, Vol. 27, No. 3, 1999, pp. 262–272.

[10]Zilliac, G.G., Degani, D. and Tobak, M., "Asymmetric vortices on a slender body of revolution," *AIAA Journal*, Vol. 29, No. 5, May. 1991, pp. 667–675.

[11]Nelson, R.C., Corke, T.C., and Matsuno, T., "Visualization and control of forebody vortices," The 12th International Symposium on Flow Visualization, Sep. 10-14, 2006, Gottingen, Germany, pp. 1-11.